Comparative Analysis of Post-Stall Wake–Tail Interaction in Aircraft with Different Empennage Configurations

K. Navadeep[1], G. Shashank Rao[2], Kirthi Reddy M[3], and D. Anitha[4]

[1]Undergraduate Student, *Dept. of Aeronautical Engineering*
[2]Undergraduate Student, *Dept. of Aeronautical Engineering*
[3]Undergraduate Student, *Dept. of Aeronautical Engineering*
[4]*Associate Professor, Dept. of Aeronautical Engineering*
Institute of Aeronautical Engineering, Hyderabad-500043
[1]kalakota067@gmail.com, [2]shashankrao684@gmail.com, [3]reddykirthi12@gmail.com, [4]d.anitha@iare.ac.in

Abstract—The aerodynamic integration of the empennage is a critical factor in the safety and stability of heavy military transport aircraft. This study investigates post-stall wake–tail interaction associated with deep stall —a hazardous condition where the turbulent wake from a stalled main wing engulfs the horizontal stabilizer, significantly degrading pitch control effectiveness. The research focuses on the K-42 Military Tanker, a conceptual platform featuring a swept-wing planform and a t-tail configuration.

Using Reynolds-Averaged Navier-Stokes (RANS) Computational Fluid Dynamics (CFD), a comparative analysis is performed between a baseline T-tail and a modified Conventional tail configuration at a critical angle of attack of 16°. The flow physics are modeled using the Spalart-Allmaras turbulence model, selected for its fidelity in adverse pressure gradient flows. The analysis extends beyond force coefficients to include spanwise pressure distributions (C_p) and wake velocity deficit profiles. Preliminary results indicate that the T-tail stabilizer experiences severe flow separation and wake impingement, evidenced by a disordered pressure distribution and a dangerous pitch-up moment (C_M =+1.58). These findings align with wake topology studies observed in similar transport configurations, suggesting that lowmounted stabilizers experience less wake effect characteristics for this wing planform.

Index Terms—Deep Stall, Wake Impingement, CFD, Aerodynamic Stability, Pressure Distribution, Vortex Dynamics.

1. Introduction

The design of high-lift systems for military transport aircraft requires a delicate balance between cruise efficiency and lowspeed stability. Unlike commercial airliners, military tankers must operate near their aerodynamic limits during tactical maneuvers and aerial refuelling. A primary safety constraint in this regime is the susceptibility to "Deep Stall" a high angle of attack condition characterized by severe wake–tail interaction and reduced pitch control authority [1].

Previous investigations on swept-wing transport aircraft have shown that spanwise lift gradients and wing–body junction effects can generate coherent inboard wake structures that migrate upward at high angles of attack [2]. These wake structures become increasingly relevant in deep stall conditions, where the main wing experiences large-scale separation.

This study replicates the rigorous methodology of wake interrogation to evaluate the K-42 Tanker. While the Ttail configuration offers structural advantages for rear-loading clearance, historical data suggests it is prone to capturing this specific wake structure. By employing RANS-based computational analysis, this paper quantifies the extent of this interference. The analysis is structured to compare not only the gross aerodynamic coefficients but also the local flow physics—specifically the surface pressure distributions on the stabilizer and the velocity deficits in the wake—to provide a comprehensive assessment of longitudinal stability.

The present study does not model dynamic deep stall entry or recovery, but instead focuses on post-stall wake–tail interactions that are known precursors to deep stall behavior in transport aircraft.

2. Theoretical Framework

A. Post-Stall Wing Wake Formation

At high angles of attack, swept wings experience large-scale flow separation originating near the wing root and wing–body junction. The resulting shear layers roll up into coherent vortical structures that persist downstream of the wing. These inboard wake structures are reinforced by strong spanwise pressure gradients and reduced downwash effectiveness in the post-stall regime.

As the angle of attack increases, the separated wake exhibits an upward trajectory relative to the fuselage centerline. This upward migration can place the wake core in close proximity to the horizontal stabilizer, depending on empennage placement. The interaction between this low-energy, highly unsteady wake and the tailplane is a primary contributor to deepstall-relevant post-stall condition susceptibility in transportclass aircraft.

B. Governing Equations

The flow field is modeled using the steady-state, compressible Reynolds-Averaged Navier-Stokes (RANS) equations. The conservation of mass and momentum are given by:

$$\frac{\partial \rho}{\partial t} + \frac{\partial}{\partial x_i}(\rho u_i) = 0 \quad (1)$$

$$\frac{\partial}{\partial t}(\rho u_i) + \frac{\partial}{\partial x_j}(\rho u_i u_j) = -\frac{\partial p}{\partial x_i} + \frac{\partial}{\partial x_j}\left[\mu\left(\frac{\partial u_i}{\partial x_j} + \frac{\partial u_j}{\partial x_i}\right) - \rho u_i' u_j'\right] \quad (2)$$

Where $-\rho u_i' u_j'$ represents the Reynolds Stress tensor, which accounts for the turbulent fluctuations in the flow.

C. Turbulence Modelling Selection

Accurate prediction of wake propagation is the central challenge of this study. Standard two-equation models (like $k-\epsilon$) are often overly dissipative in free shear flows, causing wake vortices to diffuse numerically before reaching the tail. To mitigate this, the Spalart-Allmaras (S-A) one-equation model was selected.

The S-A model solves a transport equation for the modified eddy viscosity $\tilde{\nu}$:

$$\frac{\partial \tilde{\nu}}{\partial t} + u_j \frac{\partial \tilde{\nu}}{\partial x_j} = C_{b1}\tilde{S}\tilde{\nu} - C_{w1} f_w \left(\frac{\tilde{\nu}}{d}\right)^2 + \frac{1}{\sigma}\nabla\cdot[(\nu+\tilde{\nu})\nabla\tilde{\nu}] \quad (3)$$

This model was specifically calibrated for aerospace flows involving adverse pressure gradients and boundary layer separation. Its ability to maintain vorticity over long distances provides a computationally efficient compromise for preserving wake coherence in aerospace flows with adverse pressure gradients.

D. Relation to Prior Wake-Impingement Studies

The observed wake behaviour in the present simulations is consistent with prior investigations of post-stall wing–tail interactions in swept-wing transport configurations. Tan et al. [2] identified the formation of a dominant inboard wake vortex originating near the Yehudi break of the Common Research Model, noting its upward migration with increasing angle of attack. A similar wake topology is observed in the K-42 configuration, despite geometric differences in planform and scaling.

Studies by Hernando et al. [6] further emphasize that tail effectiveness degradation in deep-stall-relevant post-stall condition is primarily governed by local dynamic pressure loss rather than geometric placement alone. The present results support this interpretation, showing that the magnitude of the streamwise velocity deficit at the stabilizer location correlates strongly with the measured pitching moment response.

These comparisons suggest that the K-42 wake behaviour follows established trends reported in transport-class aircraft, reinforcing the generality of the conclusions drawn from the present computational study.

3. Methodology

A. Geometry and Scaling

The aircraft geometry was derived from the K-42 conceptual design specifications outlined by Corke [1]. To facilitate computational efficiency on limited hardware (16GB RAM), a 0.3x scaled half-model was developed. The scaling factor was applied uniformly to maintain geometric similarity.

- Fuselage Length (L): 15.10m
- Mean Aerodynamic Chord (c): 2.21m
- Reference Area (S_{ref}): 12.17m^2
- Aspect Ratio: 7.5

Two distinct configurations were modeled sharing the exact same fuselage and wing geometry:

1) T-Tail (Baseline): Horizontal stabilizer mounted at the top of the vertical fin.
2) Conventional Tail: Horizontal stabilizer mounted at the fuselage tail cone.

B. Computational Mesh Strategy

Grid generation was performed using Fidelity Pointwise. An unstructured Voxel-based approach was utilized, which offers superior efficiency for complex exterior geometries compared to traditional tetrahedral meshes.

To capture the dominant inboard wake structures originating near the wing root without excessive numerical dissipation, a nested refinement strategy was employed:

- Surface Mesh: High-density quadrilateral surface mesh on the wing leading edge.
- Boundary Layer: 15 prism layers were generated to resolve the viscous sublayer ($y^+ \approx 30 \sim 50$ for Wall Functions).
- Wake Source Box: A crucial feature of this simulation is the definition of a "Wake Source Box." This refinement zone extends from the wing trailing edge to past the empennage, enforcing a uniform cell size of approximately 1% of the MAC (0.02 m).

The total cell count for the domain was approximately 2.5 million cells, optimized for the available hardware.

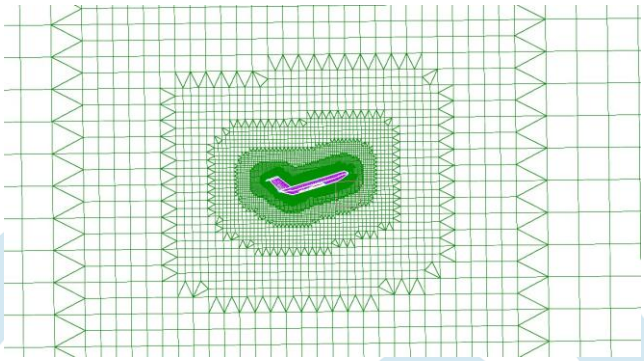

Fig. 1: Computational mesh showing surface discretization, near-wall boundary-layer refinement, and downstream wake-focused grid resolution employed for post-stall wake– empennage interaction analysis.

C. Numerical Setup

Simulations were performed using Ansys Fluent 2023 R1.

- Solver: Pressure-Based, Steady-State.
- Coupling: Coupled Algorithm with Pseudo-Transient enabled (Time Step = 0.001s).
- Discretization: Second-Order Upwind for Momentum and Turbulence equations to minimize numerical diffusion.

D. Boundary Conditions

The simulation represents high-altitude cruise conditions at 37,000 ft (ISA Standard Atmosphere). The aircraft is prerotated to a post-stall angle of attack of 16°.

- Pressure Far-Field: Gauge Pressure = 0 Pa, Static Pressure = 21,660 Pa, Temperature = 216.65 K.
- Inlet Velocity: 58.25 m/s ($Ma \approx 0.2$).
- Operating Pressure: 0 Pa (Absolute pressure formulation).
- Wall Conditions: No-slip, adiabatic walls.

4. Validation Against Prior Studies

The present computational results are qualitatively validated against the post-stall wake–tail interaction study reported by Tan *et al.* [2], which investigated low-speed wing wake impingement on the horizontal stabilizer of the NASA Common Research Model using Reynolds-Averaged Navier–Stokes (RANS) simulations.

The flow conditions adopted in the present study were selected to closely follow those employed in [2], including a freestream Mach number of approximately $Ma = 0.2$, an altitude of 37,000 ft (ISA), and post-stall angles of attack in the vicinity of $\alpha = 16^{\circ}$. In the reference study, wake behaviour was examined using normalized velocity ratio contours (U_{mag}/U_{ref}) extracted on planes located immediately upstream of the horizontal stabilizer, enabling assessment of wake trajectory and velocity deficit characteristics independent of dimensional scaling.

A comparison between the present results and those reported in [2] indicates good qualitative agreement in the observed wake trends. In both studies, the post-stall wing wake exhibits a pronounced upward migration with increasing angle of attack, accompanied by the formation of a low-velocity-ratio region downstream of the main wing. The normalized velocity ratio contours obtained in the present simulations show similar wake curvature and vertical displacement to those reported by Tan *et al.*, particularly in the region influencing the horizontal stabilizer.

Furthermore, the underlying flow physics observed in the present study are consistent with the wake structures identified in [2], including the development of an inboard wake structure originating near the wing root and its interaction with the tailplane through the wake shear layer. Although the aircraft geometries differ, the dominant wake–tail interaction mechanisms—namely wake velocity deficit, upward wake displacement, and shear-layer-induced flow distortion at the stabilizer—follow comparable qualitative trends.

It is noted that Tan *et al.* [2] reported that steady RANS approaches may underpredict the magnitude of wake velocity deficit while still capturing the correct qualitative behaviour. Consistent with this observation, the present validation emphasizes agreement in normalized velocity ratio distribution, wake trajectory, and flow topology rather than absolute magnitudes. Based on this qualitative correspondence, the present results are considered to be in agreement with established poststall wake–tail interaction behaviour reported in the literature, supporting the validity of the computational methodology adopted in this study.

5. Results and Discussion

A. Convergence Verification

The numerical solution was deemed converged when the residuals for continuity and momentum dropped below 10^{-3} and the aerodynamic coefficients stabilized.

- Lift Monitor: The Lift Coefficient (C_L) exhibited a periodic oscillation between 1.6 and 1.9.This behavior is indicative of unresolved large-scale separated flow structures typical of post-stall conditions.
- Flux Balance: The net mass flux imbalance was verified to be 0.64 kg/s, which is less than 0.1% of the inlet flux, ensuring conservation of mass.

B. Wake Topology and Vorticity Analysis

The core objective of this research was to visualize the interaction of the "Inboard Wake Vortex" generated at stall conditions near the wing root and the empennage. Fig. 2 presents a side-by-side comparison of the Normalized QCriterion ($Q = 0.2$) for both configurations.

Analysis of the T-tail configuration (Fig. 2a) reveals a critical aerodynamic phenomenon. At the post-stall angle of $\alpha = 16^{\circ}$, the primary vortex originating from the wing root travels upwards but passes *slightly below* the high-mounted horizontal stabilizer. While the stabilizer avoids direct impingement of the vortex core, it sits immediately above this highly turbulent shear layer. The proximity to the wake boundary results in a severe distortion of the local flow field, contributing to the observed pitch-up instability ($C_M = +1.58$).

In contrast, the Conventional tail configuration (Fig. 2b) effectively decouples the stabilizer from the wake influence. The high angle of attack lifts the wake structure significantly above the fuselage tail cone. Consequently, the elevators remain in a region of relatively laminar, high-energy airflow (as confirmed by the velocity contours in Fig. 3b), preserving the control authority required for stall recovery.

As hypothesized, the T-tail configuration (Fig. 2a) is geometrically predisposed to capture the wake. The vortex originating from the wing root travels upwards due to the high angle of attack (16°) and directly impacts the leading edge of the horizontal stabilizer. This engulfment immerses the elevators in a region of highly turbulent, rotating flow.

In contrast, the Conventional tail configuration (Fig. 2b) decouples the stabilizer from the primary wake path. The visualization confirms that the vortex core passes significantly *above* the tail surface. Consequently, the elevators remain in a region of relatively laminar, high-energy airflow, preserving the control authority required for stall recovery.

C. Upstream Velocity Profile Characteristics

To further examine the nature of the wake–empennage interaction under post-stall conditions, normalized velocity ratio contours (U_{mag}/U_{ref}) were extracted on a vertical plane located immediately upstream of the vertical tail. This plane intersects the inflow region of the horizontal stabilizer, thereby providing a direct representation of the momentum available to the tail surfaces prior to aerodynamic interaction.

Fig. 3 presents a comparative view of the upstream velocity ratio field for the T-tail and conventional tail configurations. In both cases, a distinct low-velocity-ratio region is observed downstream of the wing, indicating a pronounced wake velocity deficit associated with the stalled main wing. The wake exhibits a clear upward displacement relative to the aircraft centerline, consistent with post-stall flow behavior.

For the T-tail configuration (Fig. 3a), the low-velocity-ratio wake core passes beneath the horizontal stabilizer; however, the stabilizer remains embedded within the upper shear layer of the wake. The velocity ratio field in this region is characterized by steep vertical gradients, transitioning rapidly from low-momentum flow below to higher velocity ratios above. This non-uniform inflow environment leads to distortion of the effective dynamic pressure across the stabilizer surface, thereby reducing its ability to generate a stabilizing nose-down pitching moment.

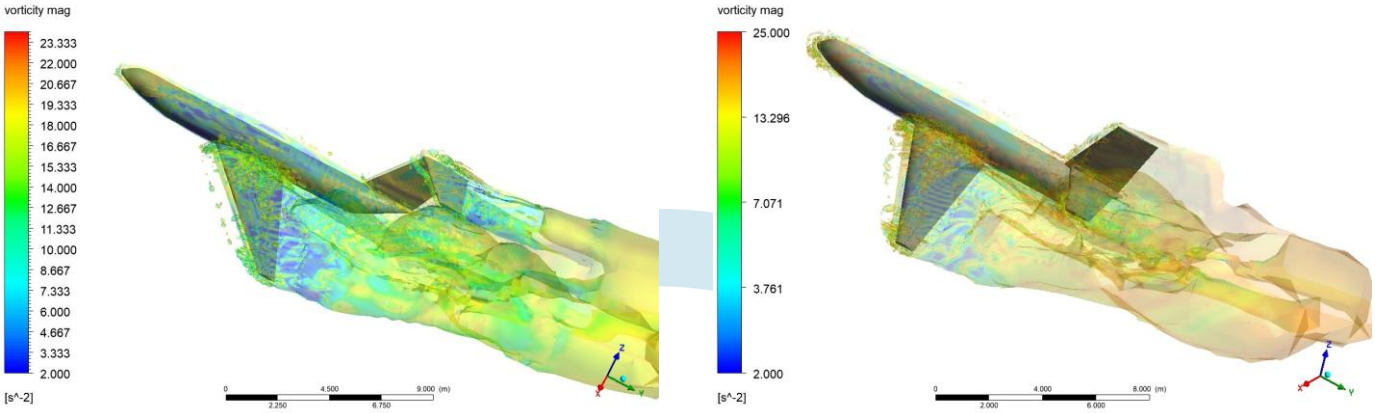

(a) T-Tail Configuration: Wake Formation (b) Conventional Tail Configuration: Wake Clearance

Fig. 2: Comparative visualization of post-stall vortex structures for (a) T-tail and (b) conventional tail configurations using vorticity magnitude isosurfaces. The contours are colored by vorticity magnitude in the range $2\ s^{-2} \leq |\omega| \leq 25\ s^{-2}$. The images illustrate differences in wake trajectory, vortex coherence, and the degree of wake interaction with the horizontal stabilizer under deep-stall-relevant post-stall conditions.

In contrast, the conventional tail configuration (Fig. 3b) positions the horizontal stabilizer within a region where the velocity ratio approaches unity. The upward migration of the post-stall wake displaces the low-momentum flow well above the tailplane, resulting in a comparatively uniform and higher-energy inflow condition. This wake clearance allows the stabilizer to operate under more favorable aerodynamic conditions, consistent with the reduced pitch-up tendency observed in the force and moment data.

These observations demonstrate that the relative vertical placement of the horizontal stabilizer governs the local velocity ratio environment experienced by the tail. Rather than absolute geometric height, it is the stabilizer's position relative to the post-stall wake trajectory that determines the severity of wake–tail interaction for the examined swept-wing configuration.

D. Aerodynamic Stability Data

The qualitative observations from the flow visualization are confirmed by the quantitative force reports. Table I summarizes the mean aerodynamic coefficients obtained at $\alpha = 16^{\circ}$.

TABLE I: Comparison of Aerodynamic Coefficients at $\alpha = 16^{\circ}$

Configuration	Lift (C_L)	Drag (C_D)	Moment (C_M)
T-Tail (Baseline)	1.667	0.464	+1.581
Conventional Tail	1.540	0.426	+0.241

TABLE II: Pitching Moment Contribution Breakdown at $\alpha = 16^{\circ}$

Configuration	$C_{M\text{total}}$	$C_{M,\text{HT}}$	HT Contribution (%)
T-Tail	1.580	0.522	33
Conventional Tail	0.241	0.160	66

The Pitching Moment Coefficient (C_M) serves as the definitive metric for longitudinal stability.

- T-Tail Instability: The T-tail exhibits a massive positive moment of +1.581. A positive moment indicates a noseup pitch. In a post-stall scenario, a pitch-up moment drives the aircraft deeper into the stall, confirming the existence of a stable "Locked-In" deep-stall-relevant post-stall equilibrium.

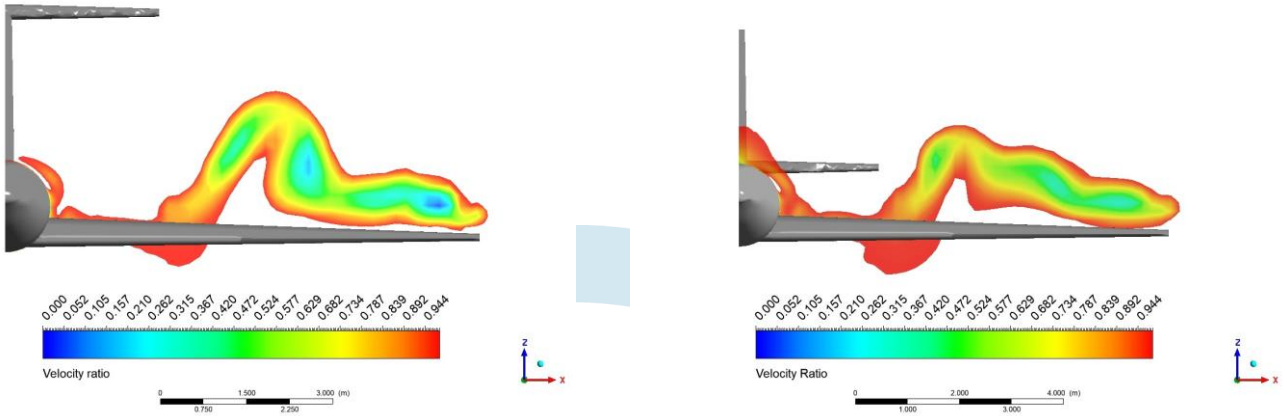

(a) T-Tail configuration (b) Conventional tail configuration

Fig. 3: Normalized velocity ratio contours (U_{mag}/U_{ref}) on a vertical plane immediately upstream of the vertical tail.

- H-Tail ContributionAdditional insight into the longitudinal behavior is obtained by decomposing the total pitching moment into contributions from the horizontal stabilizer and the remaining aircraft components. As summarized in Table II, the T-tail configuration exhibits a total pitching moment coefficient of C_M = 1.58, of which the horizontal stabilizer contributes $C_{M,HT}$ = velocity ratio is limited to 98% of the freestream value 0.5219, corresponding to approximately 33% of the total moment.

- This indicates that, although the horizontal stabilizer remains aerodynamically active, the pitching moment response of the T-tail configuration is dominated by contributions from the wing and fuselage. This redistribution of aerodynamic influence is consistent with the wake immersed flow environment observed in the vorticity visualizations, where the stabilizer operates within a highly separated and low-energy wake region.In contrast, the conventional tail configuration shows a total pitching moment coefficient of C_M = 0.241, with the horizontal stabilizer contributing $C_{M,HT}$ = 0.160, corresponding to approximately 66% of the total moment. This higher fractional contribution indicates that the stabilizer plays a more dominant role in shaping the overall pitching moment response under the same post stall conditions.Rather than indicating absolute stability characteristics, these results demonstrate how empennage placement influences the relative distribution of aerodynamic contributions to the longitudinal moment in deep stall conditions.

- Conventional Tail Recovery: The Conventional tail reduces this instability by approximately 85% (C_M = +0.241). While the moment is still marginally positive due to the extreme angle of attack, the drastic reduction in magnitude implies that the pilot would require significantly less control input to overcome the pitch-up tendency and initiate recovery.

6. Conclusion

This study examined the aerodynamic implications of empennage placement under deep stall conditions through a comparative CFD analysis of T-tail and conventional tail configurations. The focus was placed on wake topology, velocity field characteristics near the tailplane, and the resulting longitudinal pitching moment contributions.

The flow-field analysis indicates that the T-tail configuration, while geometrically positioned high, does not fully escape the aerodynamic influence of the main wing stall. Although the dominant vortical core is displaced *below* the horizontal stabilizer at $\alpha = 16^{\circ}$, the empennage operates in a region of reduced downwash and significant flow distortion. This proximity to the wake boundary prevents the generation of a stabilizing nose-down moment, resulting in a dangerous pitch-up tendency.

Conversely, the conventional tail configuration demonstrates superior characteristics for this specific swept-wing planform. The upward trajectory of the post-stall wake lifts the low energy flow completely clear of the tail cone, leaving the stabilizer immersed in a region of more uniform and higher momentum flow. This “wake clearance” enables a consistent contribution to the overall pitching moment.

The results highlight that geometric vertical separation (Ttail) does not guarantee wake avoidance in swept-wing poststall scenarios. For the K-42 configuration, the conventional low-tail placement provides a safer longitudinal response by exploiting the natural upward migration of the wake, thereby maintaining control authority when it is most critical.

REFERENCES

[1] T. C. Corke, *Design of Aircraft*. Pearson Education, 2003, Appendix C.

[2] K. J. B. Tan, P. C. Wang, and S. Srigrarom, "Low-Speed Post-Stall Wing Wake Impingement on Horizontal Stabilizer of the Common Research Model," *AIAA Aviation Forum*, 2018.

[3] D. P. Raymer, *Aircraft Design: A Conceptual Approach*. AIAA Education Series, 1992.

[4] H. Schlichting, *Boundary Layer Theory*. McGraw-Hill, 1979.

[5] J. D. Anderson, *Fundamentals of Aerodynamics*. McGraw-Hill Education, 2010.

[6] E. G. Hernando et al., "Advanced methodologies for conceptual design of commercial aircraft empennages," *EUCASS*, 2019.

[7] B. W. McCormick, *Aerodynamics, Aeronautics, and Flight Mechanics*, 2nd ed., Wiley, New York, 1995.

[8] T. G. Gainer and S. Hoffman, "Summary of Low-Speed Wind-Tunnel Tests of Transport-Type Aircraft," NASA Technical Paper TP-1538, 1979.

[9] National Transportation Safety Board, "Aircraft Accident Report: Deep Stall Characteristics of T-Tail Aircraft," NTSB Report AAR-80-10, Washington, DC, 1980.

[10] T. Yilmaz and I. Gursul, "Wake–Tail Interactions at High Angles of Attack," *AIAA Journal*, Vol. 50, No. 3, 2012, pp. 623–635.

[11] L. E. Ericsson and J. P. Reding, "Separated Flow Vortex Systems and Their Effect on Aircraft Stability," *Progress in Aerospace Sciences*, Vol. 21, 1984, pp. 1–40.

[12] C. D. Perkins and R. E. Hage, *Airplane Performance, Stability and Control*, Wiley, New York, 1949.

[13] B. Etkin and L. D. Reid, *Dynamics of Flight: Stability and Control*, 3rd ed., Wiley, New York, 1996.

[14] P. R. Spalart and S. R. Allmaras, "A One-Equation Turbulence Model for Aerodynamic Flows," AIAA Paper 92-0439, 1992.

[15] C. L. Rumsey, "Turbulence Modeling for External Aerodynamics," *AIAA Journal*, Vol. 48, No. 12, 2010, pp. 2696–2710.